ELECTRICAL SYSTEM FAULT DIAGNOSIS USING INFRARED THERMOGRAPHY

Aswin .N.B*

ABSTRACT

This project deals with the problems involved in the maintenance of electrical equipment. Improper maintenance of electrical equipments leads to lot of accidents in the workplaces. Even though there are many ways to avoid these accidents, it is not possible due to the shortage of experts. So infrared thermography is used to point out the faults in the electrical equipment. It is a non-destructive technique to point out the fault in the equipment .In our automatic diagnosis software the problematic area is captured using thermal camera .First, the algorithm will look for any repeated objects are present or not in the problematic area using invariant feature detection algorithms like Scale Invariant Feature Transform (SIFT), Speeded Up Robust Feature Transform (SURF). The result of each algorithm is compared and the best one will be considered. With the help of above result and binarization, the Region of Interest (ROI) is identified and it is segmented. The real temperature of ROI is measured using temperature software and will be given as one of the parameter input for the fault classification process, which will be done in the next phase. This algorithm will helpful to identify and classify the faults in less time, so that diagonization will be done effectively.

* Electronics and Communication Department, Sri Shakthi Institute of Engineering and Technology, Coimbatore

1.INTRODUCTION

In the power system, there are lot of electrical equipments such as circuit-breaker, transformer, lightning arrester, capacitor, potential transformer, bushing, insulator and so on. These equipments play an important role in power-supply system. Unfortunately some faults often happen to the electrical equipments because of a variety of reasons. Therefore a great cost is paid for preventive test to remove hidden dangers in power system. In recent year's infrared thermography technique were used to diagnose faults in the electrical equipments. By means of getting the thermography of electrical equipments without touching, one can judge whether the equipments is in good condition or not by analyzing the thermal distribution of the equipments. The faults of the electrical Equipments can be classified in to external and internal faults. Asfar as infrared thermography diagnosis, the external faults show mainly the overheat of connectors and they are easy to be find out. But the internal faults are difficult to be penetrated because internal faults are much more complex. To find out the internal faults, one must know the law of the internal faults attribute to the relation of their infrared thermography characteristics. The internal faults of *the* electrical equipments can be divided into loose connection or contact of internal conductors and inferiority insulation and other faults. In order to know the law of infrared thermography diagnosis we sum up a few technical problems of infrared thermography diagnosis to the electrical equipments, with internal fault and show some typical examples of thermography electrical equipments with internal fault.

2. INPUT IMAGING

The input image is the infrared image that is obtained from the thermal camera during inspection. When Thermal images are captured inappropriately, the image color can appear to be too bright or too dark and monotonous. These thermal images with flaws tend to increase the amount of mistakes inspectors made by making wrongful judgments during an inspection. Inorder to avoid this; it suggested that thermal images that do not show vivid distinction between the main objects and their backgrounds must be not included in an inspector report. Thermal images or thermograms are actually visual displays of the amount of infrared energy, transmitted and reflected by an object. Because there are multiple sources of the infrared energy, it is difficult to get an accurate temperature of an object using this method thermal

imaging is capable of performing algorithm to interpret that data and build an image. Although the image shows the viewer an approximation of the temperature at which the object is operating, the camera is actually using multiple sources of data based on the areas surrounding the object to determine that value rather than detecting the actual temperature. Thermal imaging cameras provide as with a thermogram representation in color of radiation differences in objects. Since infrared Radiation is a parameter related to temperature, a thermal inspection is used to discover differences in materials temperature. Focus is the most critical element in recording a thermal image. Focus and the perspective of the target area are the image characteristic that cannot be changed. The Infrared thermogram is usually converted in to colorful images using a color palette for human observation .images.

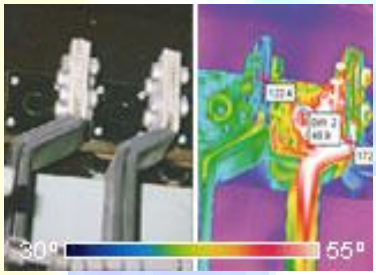

Fig.1 Images and their corresponding thermogram

BLOCK DIAGRAM OF A SYSTEM USED FOR INSPECTION EQUIPMENT

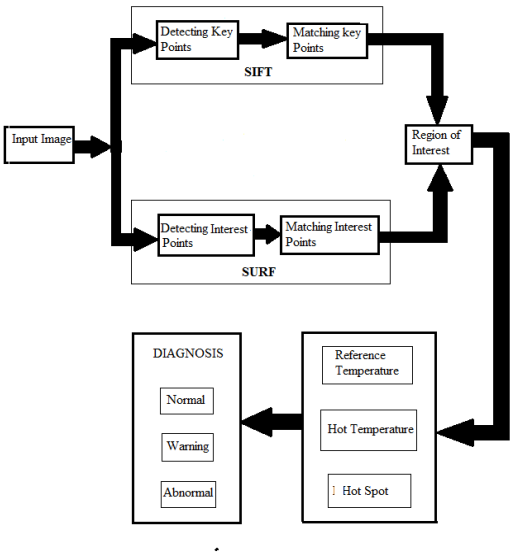

3. SCALE INVARIANT FEATURE TRANSFORM (SIFT)

3.1 Introduction

SIFT keypoints of objects are first extracted from a set of reference imagesand stored in a database. An object is recognized in a new image by individually comparing each feature from the new image to this database and finding candidate matching features based on Euclidean distance of their feature vectors. From the full set of matches, subsets of keypoints that agree on the object and its location, scale, and orientation in the new image are identified to filter out good matches. The determination of consistent clusters is performed rapidly by using an efficient hash tableimplementation of the generalized Hough transform. Each cluster of 3 or more features that agree on an object and its pose is then subject to further detailed model verification and subsequently outliers are discarded. Finally the probability that a particular set of features indicates the presence of an object is computed, given the accuracy of fit and number of probable false matches. Object matches that pass all these tests can be identified as correct with high confidence. The key stages are as follows

- Scale-invariant feature detection

- Feature matching and indexing
- Cluster identification by Hough transform voting
- Model verification by linear least squares
- Outlier detection

3.2 Scale-space extrema detection

This is the stage where the interest points, which are called keypoints in the SIFT framework, are detected. For this, the image is convolved with Gaussian filters at different scales, and then the differences of successive Gaussian-blurred images are taken. Keypoints are then taken as maxima/minima of the difference of Gaussians (DOG) that occur at multiple scales. Specifically, a DOG image is given by

$$D(x,y,\sigma) = L(x,y,k_i\sigma) - L(x,y,k_j\sigma)$$

Where $L(x,y,k\sigma)$ is the convolution of the original image I(x,y) with the gaussian blur $G(x,y, k\sigma)$ at scale $k\sigma$

$$L(x,y,k\sigma) = G(x,y,k\sigma) \times I(x,y)$$

For scale space extrema detection in the SIFT algorithm image is first convolved with Gaussian-blurs at different scales. The convolved images are grouped by octave (an octave corresponds to doubling the value of σ), and the value of k_i is selected so that we obtain a fixed number of convolved images per octave. Then the Difference-of-Gaussian images are taken from adjacent Gaussian-blurred images per octave. Once DoG images have been obtained, keypoints are identified as local minima/maxima of the DoG images across scales. This is done by comparing each pixel in the DoG images to its eight neighbors at the same scale and nine corresponding neighboring pixels in each of the neighboring scales. If the pixel value is the maximum or minimum among all compared pixels, it is selected as a candidate keypoints.This key point detection step is a variation of one of the blob detection methods developed by Lindbergh by detecting scale-space extrema of the scale normalized Laplacian that is detecting points that are local extrema with respect to both space and scale, in the discrete case by comparisons with the nearest 26 neighbours in a discretized scale-space volume. The difference of Gaussians operator

can be seen as an approximation to the Laplacian, with the implicit normalization in the pyramid also constituting a discrete approximation of the scale-normalized Laplacian. Another real-time implementation of scale-space extrema of the Laplacian operator has been presented by Lindeberg and Bretzner based on a hybrid pyramid representation.

3.3Keypoint Localization

After scale space extrema are detected (their location being shown in the uppermost image) the SIFT algorithm discards low contrast keypoints (remaining points are shown in the middle image) and then filters out those located on edges. Resulting set of keypoints is shown on last image. Scale-space extrema detection produces too many Keypoint candidates, some of which are unstable. The next step in the algorithm is to perform a detailed fit to the nearby data for accurate location, scale, and ratio of principal curvatures. This information allows points to be rejected that have low contrast (and are therefore sensitive to noise) or are poorly localized along an edge.

3.4Interpolation of nearby data for accurate position

First, for each candidate Keypoint, interpolation of nearby data is used to accurately determine its position. The initial approach was to just locate each Keypoint at the location and scale of the candidate Keypoint. The new approach calculates the interpolated location of the extremum, which substantially improves matching and stability. The interpolation is done using the quadratic Taylor expansion of the Difference-of-Gaussian scale-space function, D(x,y,σ)with the candidate Keypoint as the origin. This Taylor expansion is given by

$$D(x) = D + \frac{\partial D^T}{\partial x}x + \frac{1}{2}x^T \frac{\partial^2 D}{\partial x^2}x$$

Where D and its derivatives are evaluated at the candidate Keypoint and X=(x,y,σ)is the offset from this point. The location of the extremum, X, is determined by taking the derivative of this function with respect to X and setting it to zero. If the offset X is larger than 0.5 in any dimension, then that's an indication that the extremum lies closer to another candidate Keypoint. In this case, the candidate Keypoint is changed and the interpolation performed instead about that point. Otherwise the offset is added to its candidate Keypoint to get the interpolated estimate for the location of the extremum. A similar subpixel determination of the locations of scale-space

extrema is performed in the real-time implementation based on hybrid pyramids developed by Lindbergh and his co-workers

3.5Discarding low-contrast keypoints

To discard the keypoints with low contrast, the value of the second-order Taylor expansion D(x) is computed at the offset $\hat{x}$. If this value is less than 0.03, the candidate Keypoint is discarded. Otherwise it is kept, with final location y+$\hat{x}$and scaleσ, where y is the original location of the Keypoint at scale σ.

3.6Eliminating edge responses

The DoG function will have strong responses along edges, even if the candidate Keypoint is not robust to small amounts of noise. Therefore, in order to increase stability, we need to eliminate the keypoints that have poorly determined locations but have high edge responses. For poorly defined peaks in the DoG function, the principal curvature across the edge would be much larger than the principal curvature along it. Finding these principal curvatures amounts to solving for the Eigen values of the second-order hessian matrix, **H**

$$\mathbf{H} = \begin{bmatrix} D_{xx} & D_{xy} \\ D_{xy} & D_{yy} \end{bmatrix}$$

The eigenvalues of **H** are proportional to the principal curvatures of D. It turns out that the ratio of the two eigenvalues, say α is the larger one, and β the smaller one, with ratio r = $\frac{\alpha}{\beta}$, is sufficient for SIFT's purposes. The trace of **H**, i.e.$D_{xx}+D_{yy}$ gives us the sum of the two eigenvalues, while its determinant, i.e.,$D_{xx}D_{yy} - D_{xy}^2$, yields the product. The ratio R = $\frac{\mathrm{Tr(H)}^2}{Det(H)}$ can be shown to be equal to $\frac{(r+1)^2}{r}$, which depends only on the ratio of the eigenvalues rather than their individual values. R is minimum when the eigenvalues are equal to each other. Therefore the higher the absolute difference between the two eigenvalues, which is equivalent to a higher absolute difference between the two principal curvatures of D, the higher the value of R. It follows that, for some threshold eigenvalues ratior^{th}, if R for a candidate Keypoint is larger than $\frac{(r^{th}+1)^2}{r^{th}}$, that Keypoint is poorly localized and hence rejected. The new approach uses r^{th} = 10, this processing step for suppressing responses at edges is a transfer of a corresponding approach in the Harris operator for corner detection. The difference is that the measure for thresholding is computed from the Hessian matrix instead of a second-moment matrix.

3.7 Orientation assignment

In this step, each Keypoint is assigned one or more orientations based on local image gradient directions. This is the key step in achieving invariance to rotation as the Keypoint descriptor can be represented relative to this orientation and therefore achieve invariance to image rotation. For an image sample L(x,y) at scale σ, the gradient magnitude, m(x,y), and orientation, $\theta(x,y)$, are precomputed using pixel differences:

$$m=(x,y)\sqrt{(L(x+1,y)-L(x-1,y))^2+(L(x,y+1)-L(x,y-1))^2}$$

$$\theta\,(x,y) = \operatorname{atan} 2(L(x,y+1)-L(x,y-1), L(x+1,y)-L(x-1,y))$$

The magnitude and direction calculations for the gradient are done for every pixel in a neighboring region around the Keypoint in the Gaussian-blurred image L. An orientation histogram with 36 bins is formed, with each bin covering 10 degrees. Each sample in the neighboring window added to a histogram bin is weighted by its gradient magnitude and by a Gaussian-weighted circular window with a σthat is 1.5 times that of the scale of the Keypoint. The peaks in this histogram correspond to dominant orientations. Once the histogram is filled, the orientations corresponding to the highest peak and local peaks that are within 80% of the highest peaks are assigned to the Keypoint. In the case of multiple orientations being assigned, an additional Keypoint is created having the same location and scale as the original Keypoint for each additional orientation.

3.8Keypoint descriptor

Previous steps found Keypoint locations at particular scales and assigned orientations to them. This ensured invariance to image location, scale and rotation. Now we want to compute a descriptor vector for each Keypoint such that the descriptor is highly distinctive and partially invariant to the remaining variations such as illumination, 3D viewpoint, etc. This step is performed on the image closest in scale to the key point's scale. First a set of orientation histograms are created on 4x4 pixel neighborhoods with 8 bins each. These histograms are computed from magnitude and orientation values of samples in a 16 x 16 region around the Keypoint such that each histogram contains samples from a 4 x 4 sub region of the original neighborhood region. The magnitudes are further weighted by a Gaussian function with σequal

to one half the width of the descriptor window. The descriptor then becomes a vector of all the values of these histograms. Since there are 4 x 4 = 16 histograms each with 8 bins the vector has 128 elements. This vector is then normalized to unit length in order to enhance invariance to affine changes in illumination. To reduce the effects of non-linear illumination a threshold of 0.2 is applied and the vector is again normalized.

4.SPEEDED UP ROBUST FEATURES (SURF)

4.1 Introduction

The task of finding correspondences between two images of the same scene or object is part of many computer vision applications. It has been our goal to develop both a detector and descriptor. The search for discrete image correspondences, the goal of this work, can be divided into three main steps.

- First, 'interest points' are selected at distinctive locations in the image, such as corners, blobs, and T-junctions.
- Second, the neighborhood of every interest point is represented by a feature vector.
- Third, the descriptor vectors are matched between different images.

4.2 Interest Point Detectors

The most widely used detector probably is the Harris corner detector , based on the eigenvalues of the second-moment matrix. However, Harris corners are not scale-invariant. In order to overcome this concept of automatic scale selection was introduced. This allows detecting interest points in an image, each with their own characteristic scale. Then it is experimented with both the determinant of the Hessian matrix as well as the Laplacian to detect blob like structures. Mikolajczyk and Schmidt refined this method, creating robust and scale-invariant feature detectors with high repeatability, which they coined Harris-Laplace and Hessian-Laplace .They used a Harris measure or the determinant of the Hessian matrix to select the location, and the Laplacian to select the scale. Focusing on speed, Lowe approximated the Laplacian of Gaussian (LoG) by a Difference of Gaussians (DoG) filter. Several other scale-invariant interest point detectors have been proposed. They seem less amenable to acceleration though. Also, several affine-invariant feature detectors have been proposed that can cope with longer viewpoint changes. However, these fall outside the scope of this paper. By studying the

existing detectors and from published comparisons we can conclude that Hessian-based detectors are more stable and repeatable than their Harris-based counterparts. Using the determinant of the Hessian matrix rather than its trace seems advantageous, as it fires less on elongated, ill-localized structures. Also, approximations like the DoG can bring speed at a low cost in terms of lost accuracy.

4.3 Feature Descriptors

An even larger variety of feature descriptors has been proposed, like Gaussian derivatives, moment invariants, complex features, steerable filters , phase-based local features , and descriptors representing the distribution of smaller-scale features within the interest point neighborhood. The descriptor is called SIFT for short, computes a histogram of local oriented gradients around the interest point and stores the bins in a 128-dimensional vector. Various refinements on this basic scheme have been proposed. This PCA-SIFT yields a 36 dimensional descriptor which is fast for matching, but proved to be less distinctive than SIFT and slower feature computation reduces the effect of fast matching. A variant of SIFT, called GLOH, which proved to be even more distinctive with the same number of dimensions. However, GLOH is computationally more expensive. The SIFT descriptor still seems to be the most appealing descriptor for practical uses, and hence also the most widely used nowadays. It is distinctive and relatively fast, which is crucial for on-line applications. Recently, implemented SIFT on a Field Programmable Gate Array (FPGA) and improved its speed by an order of magnitude. However, the high dimensionality of the descriptor is a drawback of SIFT at the matching step. For on-line applications on a regular PC, each one of the three steps (detection, description, matching) should be faster still. The detector is based on the Hessian matrix, but uses a very basic approximation, just as DoG is a very basic Laplacian-based detector. It relies on integral images to reduce the computation time and we therefore call it the 'Fast-Hessian' detector. The descriptor, on the other hand, describes a distribution of Haar-wavelet responses within the interest point neighborhood.

4.4 Fast-Hessian Detector

We base our detector on the Hessian matrix because of its good performance in computation time and accuracy. However, rather than using a different measure for selecting the

location and the scale, we rely on the determinant of the Hessian for both. Given a point **x** = (x, y) in an image I, the Hessian matrix H(**x**, σ) in **x** at scale σ is defined as follows

$$H(x, \sigma) = \begin{bmatrix} L_{xx}(x,\sigma) & L_{xy}(x,\sigma) \\ L_{xy}(x,\sigma) & L_{yy}(x,\sigma) \end{bmatrix}$$

Where $L_{xx}(x,\sigma)$ is the convolution of the Gaussian second order derivative $\frac{\partial^2}{\partial x^2} g(\sigma)$ with the image I in point x and similarly for $L_{xy}(x,\sigma)$ and $L_{yy}(x,\sigma)$ Gaussians are optimal for scale-space analysis. In practice, however, the Gaussian needs to be discretized and cropped and even with Gaussian filters aliasing still occurs as soon as the resulting images are sub-sampled. Also, the property that no new structures can appear while going to lower resolutions may have been proven in the 1D case, but is known to not apply in the relevant 2D case. Hence, the importance of the Gaussian seems to have been somewhat overrated in this regard, and here we test a simpler alternative. As Gaussian filters are non-ideal in any case, and given Lowe's success with LoG approximations, we push the approximation even further with box filters. These approximate second order Gaussian derivatives, and can be evaluated very fast using integral images, independently of size. Scale spaces are usually implemented as image pyramids. The images are repeatedly smoothed with a Gaussian and subsequently sub-sampled in order to achieve a higher level of the pyramid. Due to the use of box filters and integral images, we do not have to iteratively apply the same filter to the output of a previously filtered layer, but instead can apply such filters of any size at exactly the same speed directly on the original image, and even in parallel. Therefore, the scale space is analyzed by up-scaling the filter size rather than iteratively reducing the image size. The following layers are obtained by filtering the image with gradually bigger masks, taking into account the discrete nature of integral images and the specific structure of our filters. At larger scales, the step between consecutive filter sizes should also scale accordingly. Hence, for each new octave, the filter size increase is doubled. Simultaneously, the sampling intervals for the extraction of the interest points can be doubled as well. As the ratios of our filter layout remain constant after scaling, the approximated Gaussian derivatives scale accordingly.

4.5 SURF Descriptor

The good performance of SIFT compared to other descriptors is remarkable. Its mixing of crudely localized information and the distribution of gradient related features seems to yield good distinctive power while fending off the effects of localization errors in terms of scale or space. Using relative strengths and Orientations of gradients reduce the effect of photometric changes. The proposed SURF descriptor is based on similar properties, with a complexity Stripped down even further. The first step consists of fixing a reproducible Orientation based on information from a circular region around the interest point. Then, we construct a square region aligned to the selected orientation, and extract the SURF descriptor from it. These two steps are now explained in turn. Furthermore, we also propose an upright version of our descriptor that is not invariant to image rotation and therefore faster to compute and better suited for applications where the camera remains more or less horizontal.

4.6 Orientation Assignment

In order to be invariant to rotation, we identify a reproducible orientation for the interest points. For that purpose, we first calculate the Haar-wavelet responses in x and y direction and this in a circular neighborhood of radius 6s around the interest point, with s the scale at which the interest point was detected. Also the sampling step is scale dependent and chosen to be s. In keeping with the rest, also the wavelet responses are computed at those current scales. Accordingly, at high scales the size of the wavelets is big. Therefore, we use again integral images for fast filtering. Only six operations are needed to compute the response in x or y direction at any scale. The side length of thewavelets is 4s.Once the wavelet responses are calculated and weighted with a Gaussian centered at the interest point, the responses are represented as vectors in a space with the horizontal response strength along the abscissa and the vertical response strength along the ordinate. The dominant orientation is estimated by calculating the sum of all responses within a sliding orientation window covering an angle. The horizontal and vertical responses within the window are summed. The two summed responses then yield a new vector. The longest such vector lends its orientation to the interest point. The size of the sliding window is a parameter, which has been chosen experimentally. Small sizes

fire on single dominating wavelet responses, large sizes yield maxima in vector length that are not outspoken. Both result in an unstable orientation of the interest region.

4.7 Descriptor Components

For the extraction of the descriptor, the first step consists of constructing a square region centered around the interest point, and oriented along the orientation selected in the previous section. For the upright version, this transformation is not necessary. The size of this window is 20s.The region is split up regularly into smaller 4 × 4 square sub-regions. This keeps important spatial information in. For each sub-region, we compute a few simple features at 5×5 regularly spaced sample points. For reasons of simplicity, we call dx the Haar wavelet response in horizontal direction and dythe Haar wavelet response in vertical direction (filter size 2s). "Horizontal" and "vertical "here is defined in relation to the selected interest point orientation. To increase the robustness towards geometric deformations and localization errors, the responses dx and dyare first weighted with a Gaussian (σ = 3.3s) centered at the interest point. Then, the wavelet responses dx and dyare summed up over each sub region and form a first set of entries to the feature vector. In order to bring in information about the polarity of the intensity changes, we also extract the sum of the absolute values of the responses, |dx| and |dy|. Hence, each sub-region has a four-dimensional descriptor vector **v** for its underlying intensity structure.

$$V= (\sum d_x, \sum d_y, \sum |d_x|, \sum |d_y|)$$

This results in a descriptor vector for all 4×4 sub-regions of length 64. The wavelet responses are invariant to a bias in illumination. Invariance to contrast (a scale factor) is achieved by turning the descriptor into a unit vector. One can imagine combinations of such local intensity patterns,resulting in a distinctive descriptor. In order to arrive at these SURF descriptors, we experimented with fewer and more wavelet features, using d2 x and d2 y, higher-order wavelets, PCA, median values, average values, etc.

5. SIMULATION RESULT

5.1 RESULT – SCALE INVARIANT FEATURE TRANSFORM ALGORITHM


Fig 5.1 Orginal ImageFig 5.2Selecting Key Point

5.2RESULT – SPEED UP ROBUST FEATURE ALGORITHM


Fig.5.3 original imageFig .5.4 Selecting Interest points

CONCLUSION

This Project proposes a simplified way to perform condition based maintanence of electrical equipment.Using this computerized method,diagnosis can be performed and an accurate result can be generated by the electrical inspectors.By using the SIFT and SURF algorithm the region of interest is segmented.By comparing these two algorithm the best ROI is selected.In the next phase the ROI for MSER algorithm is calculated.After that compare these three algorithm.Then check which algorithm will give better region of interest.Then the real temperature is measured using flir software from the region of interest.Finally Neural Network is used for the process of Decission making

REFERENCES

1. J. Martínez and R. Lagioia, "Experience performing infrared thermography in the maintenance of a distribution utility", paper 0279, 19th International Conference on Electricity Distribution, CIRED, Vienna, 21-24 May 2007.
2. R. Epperly, G. Heberlein, and L. Eads, "A tool for reliability and safety: predict and prevent equipment failures with thermography," Petroleum and Chemical Industry Conference, 1997. Record of Conference Papers. The Institute of Electrical and Electronics Engineers Incorporated Industry Applications Society 44th Annual, 1997, pp. 59-68
3. Lowe, D. G., Distinctive image features from scale-invariant key points," International Journal of Computer Vision, Vol. 60, No. 2, 91(2004).
4. R. Gupta, and S. Tuli, "Electrical approach to defect depth estimation by stepped infrared thermography," Proc. IEE Conf. Science, Measurement, and Technology, vol. 151, no. 4, July 2004, pp. 298- 304.
5. J. Snell, and J. Renowden, "Improving results of thermographic inspections of electrical transmission and distribution lines," Proc. IEEE Int. Conf. Transmission and Distribution Construction, 8-12 Oct. 2000, pp. 135-144.
6. Mohd Shawal Jadin, Soib Taib, Shahid Kabir, and Mohd Ansor Bin Yusof "Image Processing Methods for Evaluating Infrared thermographic Image of Electrical Equipments" Progress In Electromagnetics Research Symposium Proceedings, Marrakesh, Morocco, Mar. 20-23, 2011.
7. Ying-Chieh Chou Leehter Yao "Automatic Diagnosis System of Electrical Equipment using Infrared Thermography" 2009 International Conference of Soft Computing and Pattern Recognition.page155-160.
8. Mohd Shawal Jadin, Shahid Kabir, Soib Taib "Thermal Imaging for Qualitative-based Measurements of Thermal Anomalies in Electrical Components".
9. N. Otsu, "A threshold selection method from gray-level histograms," IEEE Trans. Systems, Man, and Cybernetics, vol. 9, no. 1, pp. 62-66, Jan. 1979.